(Received 4 August 2024, Accepted 11 September 2024, Scheduled 22 September 2024)

Spoof Surface Plasmon Polaritons-Based Feeder for a Dielectric Rod Antenna at Microwave Frequencies

Rishitej Chaparala[1], Shaik Imamvali[1], Sreenivasulu Tupakula[1], Krishna Prakash[2], Shonak Bansal[3], Mohd Muzafar Ismail[4,*], and Ahmed Jamal Abdullah Al-Gburi[4,*]

[1]*SRM University AP Andhra Pradesh, Department of Electronics and Communication Engineering, India*
[2]*NRI Institute of Technology, Vijayawada, Andhra Pradesh 521212, India*
[3]*Department of Electronics and Communication Engineering University Institute of Engineering, Chandigarh University, Gharuan, Mohali, India*
[4]*Center for Telecommunication Research & Innovation (CeTRI), Faculty of Electronics and Computer Technology and Engineering Universiti Teknikal Malaysia Melaka (UTeM), Jalan Hang Tuah Jaya, Durian Tunggal 76100, Melaka, Malaysia*

ABSTRACT: This work explores the potential of spoof surface plasmon polaritons (SSPPs) for effectively feeding high-frequency antennas operating in the extremely high-frequency (EHF) range. An innovative approach is introduced in this study to utilize SSPP to feed a dielectric rod antenna. The design incorporates a straightforward dielectric rod antenna fabricated using FR-4 material with a relative permittivity of 4.3. Compared to conventional tapered dielectric rod antennas and their corresponding feeding configurations, this design presents the potential benefit of achieving an improved gain of up to 16.85 dBi using a specific antenna length of $7.6\lambda_0$. Through careful design optimization, we achieved impedance matching and directional radiation characteristics at a frequency of 7.3 GHz. To validate our design and assess its performance, we conducted simulations using the CST Microwave Studio. This study aims to demonstrate the effectiveness and practicality of the proposed dielectric rod antenna with an SSPP feed.

1. INTRODUCTION

At optical frequencies, surface plasmon polaritons (SPPs) are electromagnetic excitations that occur in a two-dimensional manner at the interface between metal and a dielectric material. These excitations enable precise control and manipulation of light on a nanometre scale, offering substantial advantages in the platform of nano-optical devices and facilitating highly sensitive optical measurements. The remarkable confinement capability of SPP and the manipulation of light at sub-wavelength scales within nanoscale metallic structures have paved the way for a wide range of futuristic communication applications involving the development of nanophotonic devices. The free electrons in the metal, along with the surrounding electromagnetic fields, leads to intense field confinement at the metal/dielectric interface. Extensive theoretical and mathematical analyses have been conducted to explore the underlying principles of nano-optical devices and optical waveguides [1–4]. The advancements in sub-wavelength optics have disclosed a wide range of applications for SPP. These applications encompass a wide range of fields, such as super-resolution imaging, on-chip optical integrated circuits, bio-photonics, microscopy, data storage, photovoltaics, graphene-based devices, photolithography, molecular sensors, photocatalysis, thin-film solar cells, and resonant waveguide gratings [5–11].

To advance the progress of integrated circuits and devices operating in the microwave and terahertz frequency ranges, researchers have explored the utilization of SPP at lower frequencies. However, metals act as perfect conductors in these frequency regimes, and they cannot support SPP. To address this limitation, plasmonic metamaterials [12–15] have been proposed to enable the realization of SPP at lower frequencies. The geometrical structure of the metallic surface was textured to enable a more profound interaction between the electric field and metal. Due to their inherent 3D geometries, they face significant limitations in applications. Out of numerous SSPP structures, the ultrathin corrugated metallic strip structure with single- and double-periodic grooves stands out as highly promising, due to its straightforward planar design [16, 17].

However, operating microwave SSPP devices independently presents challenges due to inefficiencies in signal feeding and extraction. Typically, they must be integrated with conventional microwave circuits, primarily composed of transmission lines. Consequently, there is a need to efficiently convert guided waves into SSPP. Several investigations, as reported in works [18–20], have addressed the conversion from transmission lines to plasmonic devices. In work [18], corrugated grooves are utilized to establish a conversion mechanism between coplanar waveguide (CPW) and SSPP devices. Building upon this work, work [19] extends the conversion approach, with grooves protruding from the inner conductor of CPW rather than being inlaid within it. Both studies employ an exponential Vivaldi slot line for the conversion process. In contrast,

* Corresponding authors: Mohd Muzafar Ismail (muzafar@utem.edu.my), Ahmed Jamal Abdullah Al-Gburi (ahmedjamal@ieee.org).

work [20] explores an alternative approach, confining the SSPP wave between two corrugated metallic strips in opposite directions, with electromagnetic energy coupled to it via a back-end microstrip featuring a circular metal plate. Despite these advancements, current SSPP devices still exhibit imperfections. In works [18] and [19], the Vivaldi slot proves indispensable, posing complexity due to its design parameters. In work [20], the necessity of a bottom microstrip layer for electromagnetic energy coupling and an air hole at the input end of the upper slot line further complicates design and renders it impractical for microwave integrated circuits. In work [21] to mimic SPP in microwave frequency range, the concept of spoof SPP on ultrathin and flexible corrugated metallic strips has been introduced and developed. The design schemes for both passive and active devices transition to SSPP systems are respectively outlined.

These SSPPs offer benefits such as lightweight construction, conformability, low profile, and seamless integration with conventional microwave circuits. Several microwave systems utilizing SSPP are highlighted. Pendry et al. explored the remarkable capability of engineering surface plasmons across a broad range of frequencies. They demonstrated the ability to manipulate and direct radiation at surfaces, providing control over electromagnetic interactions within a wide spectral range. The use of highly conductive structured surfaces and metals controls the size and spacing of the holes to create designer surface plasmons. Although they succeeded in creating surface plasmons, they were unable to achieve the generation of SSPP [22]. Another study by Hibbins et al. investigated the pronounced localization of the electric field at the interface, as well as the curvature of the light line, known as dispersion curve. However, they did not observe the propagation of the SSPP along the interfaces [23]. Rusina et al. introduced periodic grooved structures that supported SSPP of a certain width and depth, placed in a dielectric material. Optimized parameters of the structure enable the effective guidance and confinement of light in THz fields [24]. Gao et al. designed an ultrathin dual-band plasmonic waveguide that supports two designer SSPPs. Conventional methods for feeding microstrip lines encounter challenges such as radiation losses, crosstalk, and mutual coupling, resulting in signal integrity concerns and imposing limitations on the overall performance of microwave systems. SSPP technology offers a solution to this problem by providing high confinement through wave manipulation at the sub-wavelength scale [25].

The utilization of SSPP-based feeding presents several advantages. Firstly, the SSPP design offers superior compactness compared to microstrip design. Additionally, they facilitate gain enhancement through strong field confinement. Moreover, SSPP affords tuneable properties by adjusting geometric parameters, enabling the optimization of resonance frequency and gain. Manufacturing SSPP devices is simple and cost effective. Spoof surface plasmon polaritons are artificially designed structures and plasmonic metamaterials. By mimicking the SPP propagation into the microwave and terahertz frequencies, spoof surface plasmon polaritons are introduced, which are usually generated with periodic subwavelength grooves, holes, etc. Zhang et al. proposed an efficient transition structure for trapping surface plasmon waves. This structure involves gradient corrugated grooves with an under-layer ground, which facilitates the conversion of the microstrip line to the SSPP mode. Corrugated grooves, consisting of uniform-width stubs with periodicity, enable the creation of SSPP devices. In these devices, plasmonic metamaterials contain grooved surfaces that mimic surface waves in the microwave/THz frequency range, a technique known as "spoofing" [26]. Investigations [27–29] have demonstrated that a unit cell graph contains a linear relationship between the frequency and propagation constant, with the dispersion of the straight line increasing as the groove height increases. Chaparala and Tupakula successfully employed an SSPP structure by adjusting the width of its corrugated grooves from 1 mm to 2 mm [30]. All dimensions of the SSPP waveguide remained constant [26], except for the groove width (p-a), which was adjusted from 1 mm to 2 mm. This change proved to be an effective feeding mechanism, resulting in an enhanced gain, increased by approximately 0.83 dBi compared to the existing design with a 1 mm width [30]. This adjustment spans from $h1$ to $h7$ on both sides and is then subjected to simulation. To implement the waveguide, a dielectric substrate of FR4 material with a thickness of 1.6 mm was used. The copper layer used in this experiment had a thickness of 0.035 mm with FR4 epoxy having a dielectric constant of 4.3.

As wireless devices continue to expand their frequency spectrum, the significance of antenna bandwidth has become increasingly important. This has led to growing interest in investigating ultra-wideband (UWB) antennas, which provide a wide impedance bandwidth. Several types of UWB antennas are commonly used, including log-periodic antennas, bow-tie antennas, spiral antennas, tapered dielectric rod antennas, and conventional transverse electric and magnetic (TEM) horn antennas. Among them, planar tapered dielectric rod antennas [31–38] are well-regarded for their ability to generate higher gain and greater radiated power than other antennas of the same length. These antennas also exhibit superior impedance matching, have significant potential for packing multiple elements, and experience reduced losses.

This work presents a patch-fed dielectric rod antenna based on the research conducted by Ghattas et al. Compared with conventional tapered dielectric rod antennas, this configuration exhibits higher gain capabilities. Numerous feeding techniques have been explored for dielectric rod antennas for various applications. These techniques include a patch-fed dielectric rod antenna for dual-band applications [31], a dielectric rod antenna fed by a rectangular waveguide for photo mixer-based terahertz sources [34], optimal feeding of dielectric rod antenna arrays using photonic crystal waveguides [33–35], and excitation of a planar horn antenna and patch antennas with an SSPP waveguide [36–39]. Employing the microstrip patch feeding technique leads to increased losses, which may affect the gain levels of the rod antenna. However, this is not suitable for high-frequency applications. To counteract this challenge, we introduced the SSPP feeding technique. This technique supports the propagation of high-frequency surface plasmon waves along a metal surface within a structure made with periodic grooves. Hence, the conversion of the quasi-transverse electric and mag-

netic waves of the microstrip line feeding into SSPP waves was realized within the microwave frequency spectrum.

The key advantage of the SSPP feeding technique lies in its ability to significantly reduce reflections, thereby enabling high gain. The aim of this study is to propose a novel antenna feeding structure by eliminating the patch-fed antenna excitation and applying SSPP feeding element to the rod antenna. Alternative structures, such as a 1/4 impedance transformation microstrip line or a microstrip CPW structure, can also be utilized. However, these methods do not effectively shift the operating frequency of the rod antenna from the millimetre waveband to a lower range. The unique advantage of SSPP feeding lies in its ability to achieve this frequency transition, demonstrating its superior efficacy in adjusting the operational bandwidth of dielectric rod antennas. The objective is to achieve a higher gain and better impedance match than those reported in existing studies [35–43].

The structure of the paper is organized as follows. Section 1 provides an introduction to the study. Section 2 discusses the geometrical properties of the feeder and presents an analysis of the dispersion graph. Section 3 covers the simulation studies and the optimization of the proposed SSPP-fed dielectric rod antenna. Finally, Section 4 presents the experimental results and compares them with the simulated outcomes.

2. FEEDER GEOMETRICAL PROPERTIES

This paper introduces and showcases an SSPP waveguide transition structure and its use as a feeding mechanism for the dielectric rod antenna. Fig. 1 illustrates the fabricated SSPP waveguide structure, while Fig. 2 shows the S parameters of both the simulated and measured characteristics of the SSPP waveguide. The designed waveguide structure consists of gradient grooves with heights ranging from 0.5 mm to 3.5 mm, facilitating the conversion of guided waves to SSPP.

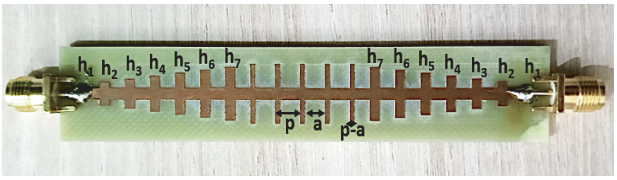

FIGURE 1. Fabricated device of a spoof surface plasmon polaritons waveguide.

Figure 2 shows the simulated and measured characteristics of the SSPP waveguide. In the simulated S-parameter characteristics in Fig. 2, the reflection coefficient S_{11} is represented by a black line, falling below -10 dB in the frequency range of 1–10 GHz. This indicates a high degree of optical confinement and impedance in the SSPP waveguide structure. In the following section, a comprehensive analysis of the patch-fed dielectric rod antenna is presented.

To achieve highly efficient and low-loss transitions, it is essential to convert the quasi-transverse electromagnetic (QTEM) mode of the microstrip to the TM modes while ensuring alignment in polarization, momentum, and impedance. The transition design, which enables the conversion of the microstrip's guided mode to the slow-wave spoof SPP surface mode, is a key to this process. This matching is smoothly accomplished by gradually altering the height of the grooves, facilitating a seamless transition between the TEM wave and slow-wave mode. Fig. 3(a) illustrates the design of this mode converter, where the groove heights increase from h_1 to h_7. As depicted in Fig. 3(b), the yellow curve represents the freely propagating wave vector (k_0), while the maroon curve denote the wave vector (k_y) for the SSPP cells. As the groove height increases, the wave vectors gradually transition from k_0 to match k_y. It demonstrates the momentum conversion at microwave frequencies, highlighting the smooth transition of the wave's momentum through the mode converter. Fig. 3(c) depicts the unit cell structure of the designed SSPP waveguide, with dimensions $W = 3$ mm, $a = 4$ mm, $p = 5$ mm, and $h = 4$ mm. Fig. 3(d) shows that the dispersion curve for SSPP (k_y) significantly diverges from the light line (k_0), indicating a momentum mismatch between these wave vectors. Therefore, achieving a highly efficient and low-loss transition requires a mode converter and matching section that align polarization, momentum, and impedance.

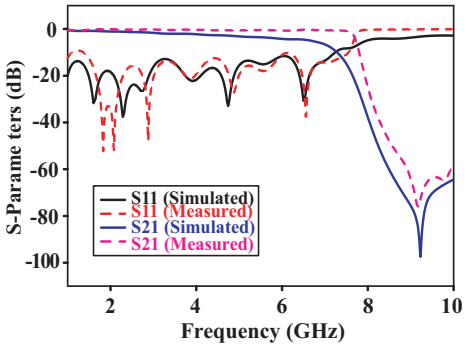

FIGURE 2. Simulated and measured characteristics of the SSPP waveguide structure.

3. SIMULATION STUDIES AND OPTIMIZATION

Figure 4 shows a schematic of the patch fed rod antenna dimensions with a specific rod length. The design features a dielectric rod antenna constructed from FR4 material, with a thickness of 1 mm and a relative permittivity of 4.3, along with a copper patch section with a thickness of 0.04 mm. The antenna was fed with a rectangular patch measuring 3×3 mm. L_1, L_2, and L_3 represent the lengths of the dielectric rod antenna along the z-axis, while D_1 and D_2 denote the dimensions along the x-axis. To enhance the gain, the top and bottom portions of the dielectric rod were tapered along the y-axis with lengths D_3 and D_4, where D_3 equals $0.08\lambda_0$, and D_4 equals $0.28\lambda_0$. This tapered section enhances the antenna's gain. The dimensions of the solid uniform sections of the dielectric rod antenna are provided in Tables 1 & 2. Each element and its dimensions

TABLE 1. Optimized measurements of the antenna.

L_1	L_2	L_3	D_1	D_2
λ_0	$6\lambda_0$	$0.6\lambda_0$	$0.2\lambda_0$	$0.6\lambda_0$

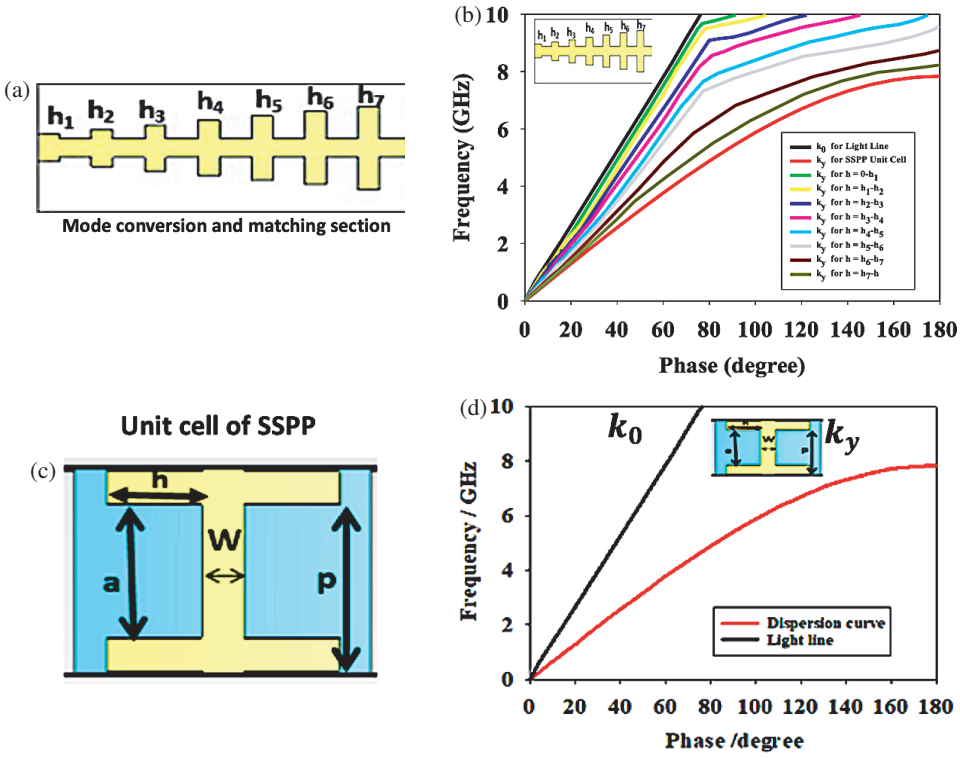

FIGURE 3. (a) and (b) Gradient grooves for mode conversion and momentum matching from guided mode to SSPP mode. (c) and (d) SSPP unit cell structure and dispersion graph related to the grove height (h) of 4 mm.

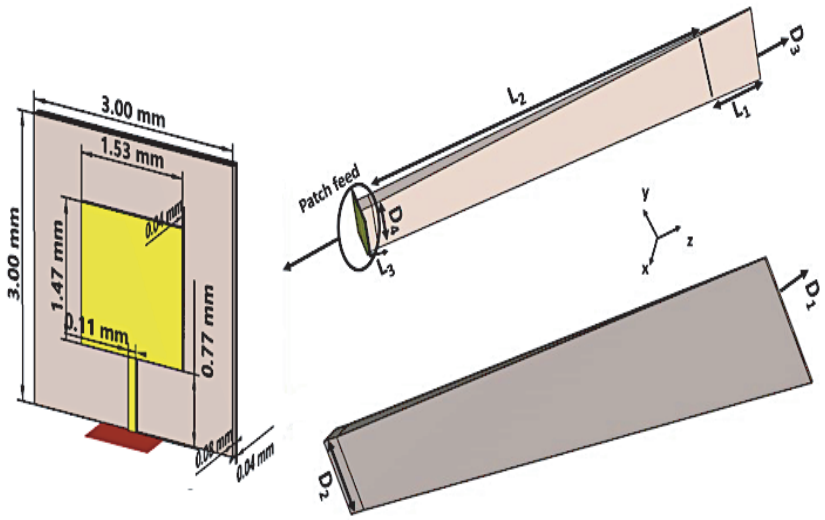

FIGURE 4. Simulated design of a patch-fed dielectric rod antenna dimensions representing the total rod length and diameter of tapering sections.

TABLE 2. Tapered rod section.

D_3	D_4
$0.08\lambda_0$	$0.2\lambda_0$

were determined to be optimal, ensuring that discrete variations in steps occurred across the length of the middle rod L_2, ranging from $2\lambda_0$ to $7\lambda_0$. This process aims to enhance gain through optimization. The dimensions are optimized such that the considered rod antenna, fed by the patch antenna, exhibits maximum gain. The response of the antenna was meticulously recorded through simulations in the frequency range of 56 to 65 GHz. Extensive simulations in the 56–65 GHz range confirmed impedance matching and optimized gain at 59.3 GHz. Fig. 5 shows the reflection coefficient comparison of single patch and dielectric rod. Using a rod, the single patch achieves an improved impedance match. Fig. 6 demonstrates the gain of the patch-fed dielectric rod antenna, which is 8.13 dBi at 59.3 GHz.

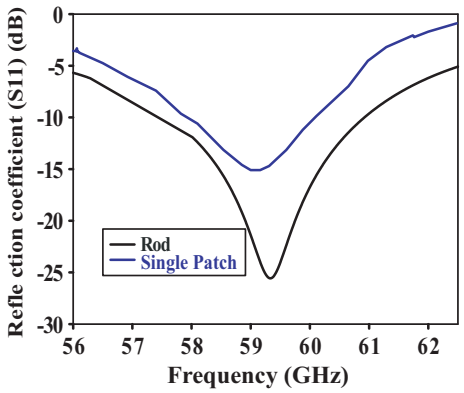

FIGURE 5. Reflection coefficient (S_{11}) comparison for single patch and dielectric rod without SSPP feeding technique.

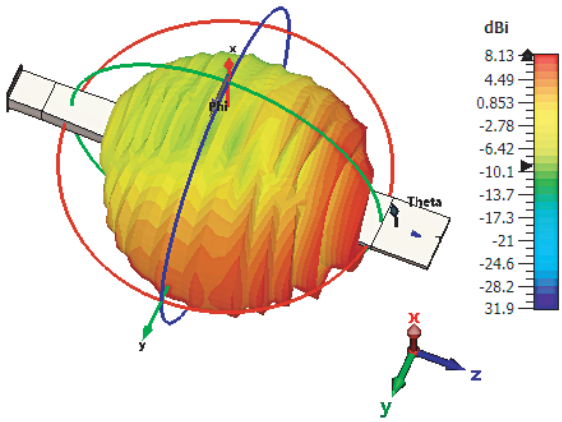

FIGURE 6. The gain of the patch-fed dielectric rod antenna at 59.3 GHz.

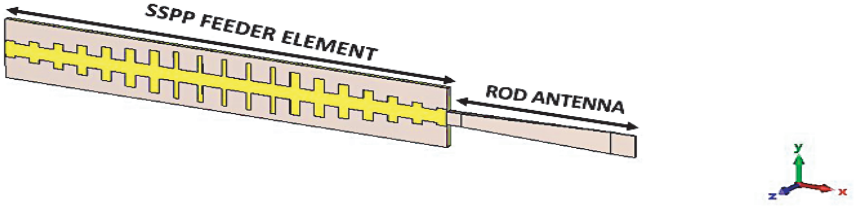

FIGURE 7. The novel feeding structure of the dielectric rod antenna with SSPP waveguide feeding.

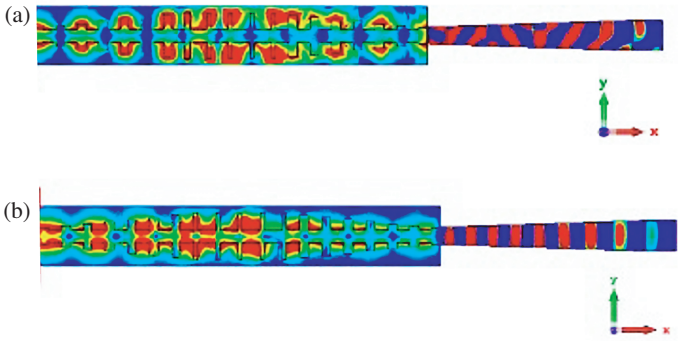

FIGURE 8. Distributed (a) E field and (b) H field radiation for designed SSPP-based dielectric rod antenna at 7.2 GHz.

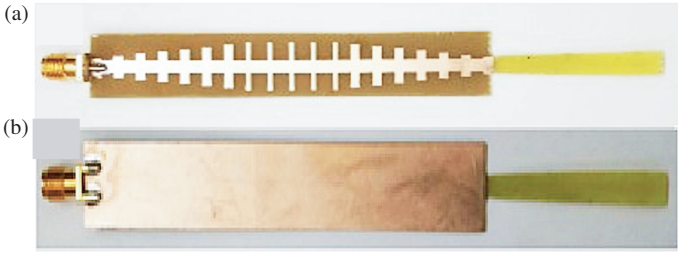

FIGURE 9. The fabrication samples of (a) front, (b) back view of the SSPP-fed dielectric rod antenna.

By utilizing the SSPP waveguide structure, the dielectric rod antenna was successfully operated within the low-frequency band. Remarkable results were achieved by integrating the SSPP waveguide with an mm-wave band dielectric rod antenna in the 1–10 GHz range. In the initial setup, the dielectric-rod antenna was fed using a microstrip patch antenna. In this study, an SSPP feeding technique was employed to excite the dielectric rod antenna without a patch. The corresponding simulation results were obtained at a frequency of 7.2 GHz. All dimensions were the same as those previously described. To achieve the proposed configuration, the patch section was removed, and feeding to the rod antenna was directly provided from the designed SSPP waveguide. Fig. 6 depicts the connection between the SSPP waveguide and antenna section. Feeding was performed across a single port at the end of the SSPP feeding structure. The other end of the SSPP feeder was connected to the load made up of the rod antenna, as shown in Fig. 7. Additionally, Figs. 8(a) & (b) display the distributed E- and H-field radiation of the designed SSPP-based feed of the dielectric rod antenna at a simulated frequency of 7.2 GHz. The feeder produces confined electromagnetic waves with the ability to stimulate a dielectric-rod antenna. These waves propagate along the x-axis, whereas the field becomes concentrated along the z-axis. Fig. 8(b) clearly shows that SSPP supports magnetic field distribution to stimulate the rod antenna over electric field distribution.

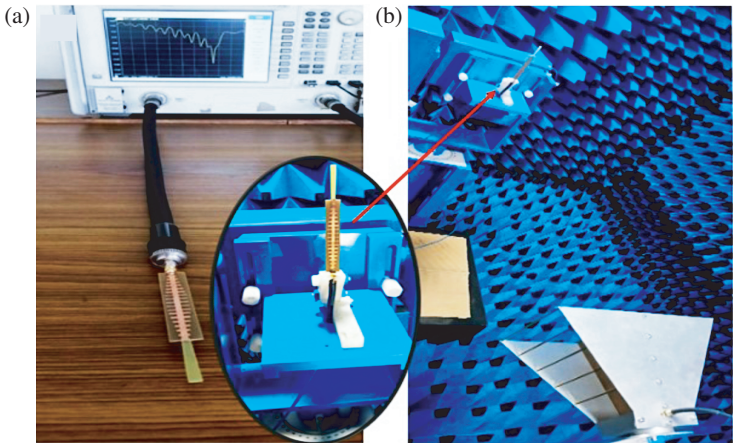

FIGURE 10. SSPP Rod antenna. (a) Measurement of S-parameters with VNA. (b) Testing SSPP Rod antenna in Anechoic Chamber.

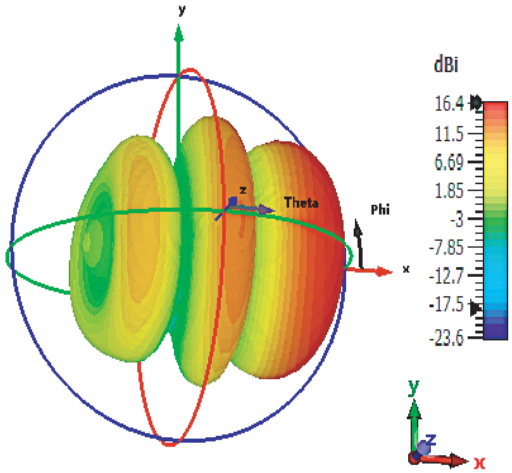

FIGURE 11. Gain of the SSPP fed dielectric rod antenna at 7.2 GHz.

4. EXPERIMENTAL CHARACTERIZATION AND RESULTS

Figure 9 illustrates the fabricated sample displaying both the front and back sides of the proposed antenna. The fabrication procedure for the proposed tapered dielectric rod antenna utilizes milling and etching technologies with an MITS PCB electronic machine, employing low-cost materials. The materials required for this process are copper and dielectric FR-4. This method is both simple and cost-effective.

CST Microwave Studio was used to conduct the simulation, while Agilent N5247A: A.09.90.02 vector analyser was employed for the measurement process. Figs. 10(a) and 10(b) show the experimental setup of the proposed configuration. Fig. 10(a) shows the reflection coefficient (S_{11}) measurement image of the designed SSPP-fed dielectric rod antenna. The measurement image was captured during the initial connection. Subsequent iterations led to improvement in the measurement setup. Fig. 10(b) shows the connected SSPP-fed dielectric-rod antenna in the anechoic chamber. Based on the simulation result presented in Fig. 11, the gain achieved was 16.4 dBi at 7.2 GHz. However, during the actual measurement shown in Fig. 10(b), the recorded gain was 16.85 dB at 7.3 GHz. Hence, the analysis of the gain in the experimental setup highlighted a noticeable peak at 7.3 GHz. Consequently, at 7.3 GHz, the measured experimental gain value of the designed SSPP-fed dielectric rod antenna and the corresponding E- and H-plane radiation patterns for the same frequency were subsequently studied. The gain of the reference antenna G_{REF} was determined using the Amkom horn antenna, which operates within the frequency range of 1–18 GHz, providing broad frequency coverage.

VNA calibration was performed using a 3.5 SMA calibration kit. The distance between antenna under test (AUT) and the reference antenna is 1.5 meters. The antenna radiation pattern plot indicates stronger radiation around 0° and 180°, with some discrepancies between the two patterns in the -10 dB to -20 dB regions, likely due to measurement or environmental variations. Overall, the agreement between the simulated and measured results validates the antenna's design, though minor real-world effects are observed, as shown in Fig. 12(a). The antenna's H-plane plot at 7.3 GHz also shows good agreement between the simulated (red) and measured (black) radiation patterns, with most energy radiated between -10 dB and -20 dB, as presented in Fig. 12(b). Moreover, the radiation patterns of the proposed configuration exhibit stability. This indicates the efficacy of the suggested feeding technique in attaining a high gain pattern of this nature. By employing the SSPP feeding structure to feed the rod antenna, an adjustment was made. This involved changing the width (W) of the grooveless metallic line at the top layer of the SSPP waveguide, and the width (W) is chosen as 3 mm, precisely aligning it with the dimension ($L_3 = 0.6\lambda_0$) of the lower rod antenna. This adjustment resulted in an improved impedance match. Although there was a slight frequency deviation resulting from the measurement error due to mismatch, the simulated (7.2 GHz) and measured (7.3 GHz) reflection coefficients (S_{11}) generally exhibited good agreement. The mismatch between simulated and measured S parameters arises due to differences in the boundaries between simulated and measured responses. The loading effect in the measurement setup differs significantly from that in the simulated case. The precision of the vector network analyser, along with the particulars of the measurement setup, crucially influences the accuracy of the measured values, particularly in determining return loss. In both the simulated and measured plots of the proposed configuration, the signal strength's reflection coefficient consistently stays below -10 dB within the 5 to 8 GHz bandwidth range. Fig. 13 depicts the results for both patch-fed and SSPP-fed configurations of the rod antenna. Compared to the patch-fed configuration, the SSPP feeding reduces the operating frequency range from 56–65 GHz to 1–10 GHz. The reduction in the operating frequency of the dielectric rod antenna when it is fed with the SSPP-based method is attributed to the principle of SSPP. SSPPs mimic high-frequency waves, enabling their propagation at lower fre-

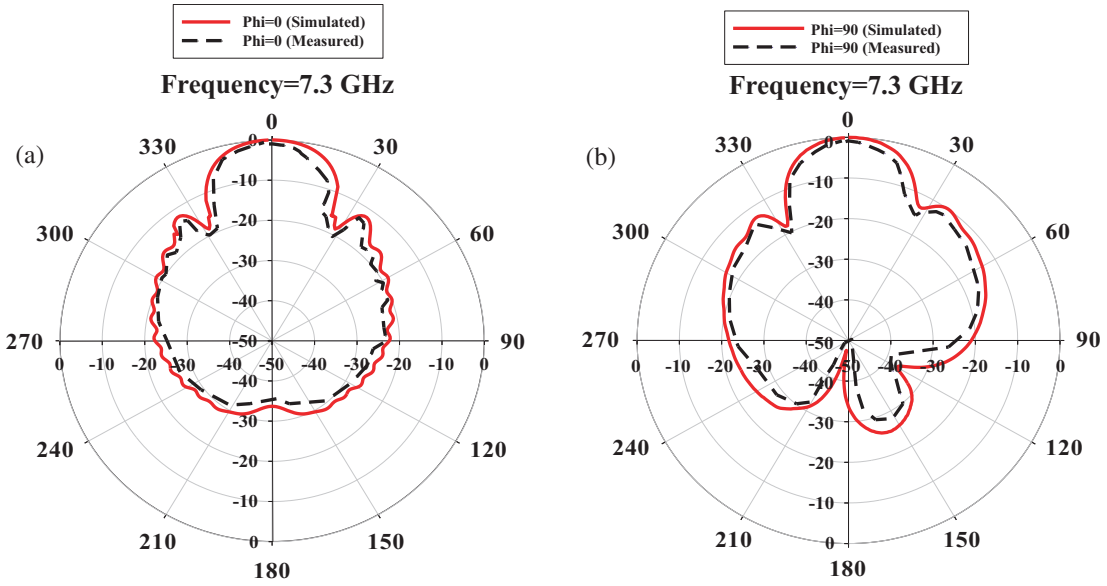

FIGURE 12. (a), (b) Represent the E and H plane patterns of the dielectric rod antenna fed by the SSPP.

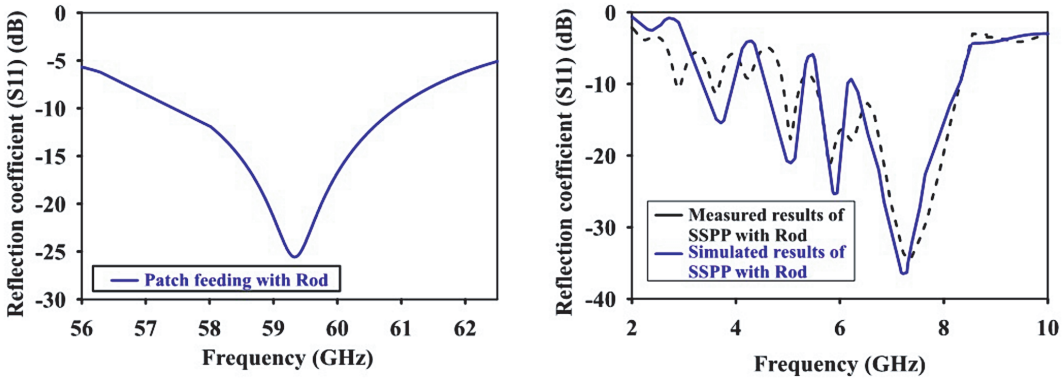

FIGURE 13. Comparison of significant results for the rod antenna without SSPP and with SSPP.

quencies. This clearly justifies the observed shift in the dielectric rod antenna's operational frequency to lower bands when SSPP feeding is applied. Natural SPPs are surface electromagnetic waves that travel along the interface between a conductor and a dielectric, tightly bound to the surface. They exist at optical frequencies. SSPPs are artificially engineered versions of SPPs that can propagate at much lower frequencies, such as microwave or terahertz, by structuring the surface of the metal.

Figure 14 shows the resulting S_{11} parameters of SSPP configurations, both with and without the rod. The curve representing SSPP fed with the rod demonstrates a broader bandwidth for impedance matching than the curve without the rod. Fig. 15 illustrates the frequency-dependent variations of the gain curve for the dielectric rod antenna fed by SSPP. The observed gain exhibited a linear relationship with the frequency. The experimental plot closely resembles the simulated one. In Fig. 16, the Voltage Standing Wave Ratio (S) is observed to decrease to approximately 1.31 at 7.2 GHz, closely matching the theoretical value of $S = 1.39$. A comparison of improvements for the proposed configuration and those of recently published works is reported in Table 3. The entries listed in Table 3 represent previously published studies cantered around diverse feeding mechanisms for the designed antennas operating across various frequencies. All the studies have a common objective of enhancing gain with improved impedance matching. In comparison, the current configuration with SSPP is capable of tightly confining the EM wave. Hence, optimal gain is achieved with decent impedance matching as evidenced by the outcomes. Notably, other feeding approaches such as coaxial line feed and planar feed methods have their limitations. Coaxial line feed poses challenges in modelling due to the need for substrate perforation, while planar feed methods are more suitable for arrays where interactions between elements and feed lines are prevalent. A drawback associated with coplanar waveguide (CPW) feeding is the limited comprehension within the microwave design community regarding its practical application.

Advantages of the proposed design over existing literature:

1. Simplified structure: The proposed structure offers a more straightforward design than 1/4 impedance transformation microstrip line or a microstrip CPW structure [35–43].

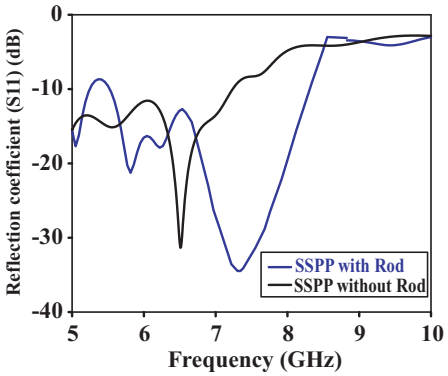

FIGURE 14. Comparison of impedance bandwidth curves of SSPP without and with rod.

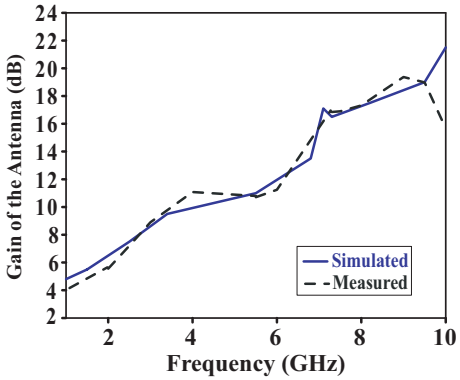

FIGURE 15. Gain Vs Frequency plot for designed SSPP-based dielectric rod antenna for both simulated and measured data.

TABLE 3. Comparison of research work with existing methods.

Ref.	Feeding source	(f_0) GHz	Gain (dBi)	S_{11} (dB)	Antenna length	Bandwidth (%)
[35]	Photonic crystal	-	13.5 dBi	-	$\lambda_0/2$	-
[36]	SSPP	6.7 GHz	8.43 dBi	−21 dB	$2\lambda_0$	6.4–6.6 GHz (0.07)
[37]	Horn	9.9 GHz	8.15 dBi	−25 dB	$5\lambda_0$	6.5–10.4 GHz (46)
[38]	SSPP	30 GHz	6.8 dBi	−18 dB	6.08 × 4.51 mm	4.2–6.5 GHz (43)
[39]	SSPP	26.18 GHz	6.1 dBi	−28.8 dB	8.3 × 2 mm	27.9–30.5 GHz (8.82)
[40]	Co axial line feed to DRW	27 GHz	14 dBi	−26 dB	$0.11\lambda_0^2$	17.9–44.1 GHz (84.5)
[41]	Planar feed DRA	16.4 GHz	16.5 dBi	−40 dB	$6.5\lambda_0$	12–16.3 GHz (29.9)
[42]	Plasmonic WG	225 THz	12.5 dBi	−28 dB	$12.78\lambda_0$	(32.55)
[43]	DRA + slot	7.6 GHz	14 dBi	−28 dB	19.3 mm	7.5–9.3 GHz (21.35)
[This work]	**SSPP**	**7.2 GHz**	**16.4 dBi**	**−36.3 dB**	**$7.6\lambda_0$**	**5.4–8.2 GHz (38.8)**

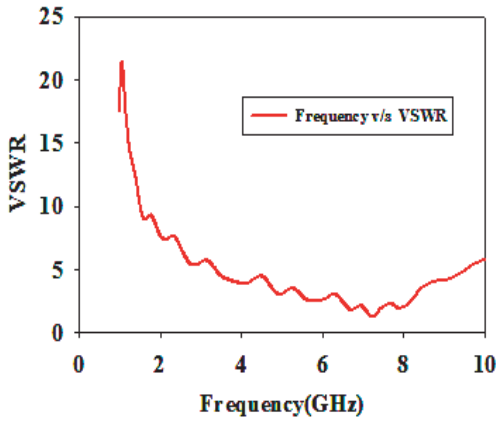

FIGURE 16. Simulated VSWR result of the proposed configuration.

2. Lower operating frequency: Due to the implementation of SSPP feeding, a dielectric rod antenna, which originally operated in the millimetre waveband, has been adapted to function within a lower frequency range of 1–10 GHz.

3. Enhanced gain: The proposed structure demonstrates improved gain over existing designs [35–43].

4. Improved impedance match: The reflection coefficient (S_{11}) of the proposed design shows enhanced matching compared to existing designs [35–43].

5. Cost effectiveness: It offers cost advantages in production, maintenance, and implementation, potentially leading to significant savings.

Limitations of the proposed design compared to existing literature:

1. Feeder length: The rod antenna's feeder in the proposed design made of SSPP has a larger length than the antenna itself.

2. Complex field interaction: Distinguishing between specific and nonspecific field interactions along the SSPP's surface is challenging.

This paper offers several significant benefits that contribute to both the academic community and practical applications:

1. Advancement of knowledge: The study offers novel insights into the SSPP concept, particularly in confining high frequency signals to low frequency operation, as outlined in the existing literature. It also presents a fresh perspective on the operation of dielectric rod antennas with SSPP feeding.

2. Practical applications: The findings can be directly applied to feed high-frequency antennas operating in the mm-

wave or optical frequency range, enabling their characteristics to be reproduced at lower frequencies. This approach can be effectively utilized in the design and integration of plasmonic waveguide circuits.

3. Methodological contributions: The innovative approach used in this research can serve as a model for future studies investigating the potential of SSPP for feeding high-frequency antennas, as detailed in this paper. The applied methodologies provided specialized expertise in antenna design, material characterization, and simulations using CST Microwave Studio.

4. Interdisciplinary applications: The SSPP feeding mechanism's compatibility with emerging technologies, such as metamaterials and nanotechnology, could drive interdisciplinary innovations in antenna design potentially leading to next-generation antennas that integrate the best features of various advanced technologies.

5. CONCLUSION

This work explains the design, development, and analysis of SSPP waveguide to feed the high frequency rod antenna. The simulations demonstrate the exceptional optical confinement of the SSPP waveguide from mm-wave band to the microwave frequency range. The waveguide's geometry, as presented in this paper, serves as the fundamental basis for developing RF front-end circuits through the utilization of designer SPP at microwave frequencies. Additionally, this waveguide structure is effectively used to feed the dielectric rod antenna offering superior impedance matching and gain compared to existing designs. The enhanced gain, improved impedance matching, and use of cost-effective materials such as FR-4 present a compelling case for high-performance, low-cost solution that revolutionizes antenna technology suitable for a wide range of applications in future wireless communication technologies. Despite the limitation of a large feeder length, this design demonstrates potential for integrating plasmonic waveguide circuits. Consequently, researchers can explore integrating multiple plasmonic devices for various applications using the technique presented in this work.

ACKNOWLEDGEMENT

The authors wish to express their profound gratitude to Universiti Teknikal Malaysia Melaka (UTeM) for their generous support. This work was made possible through the grant PJP/2024/FTKEK/PERINTIS/S01388. Their assistance and resources have been instrumental in the successful completion of this research.

REFERENCES

[1] Zayats, A. V., I. I. Smolyaninov, and A. A. Maradudin, "Nano-optics of surface plasmon polaritons," *Physics Reports*, Vol. 408, No. 3-4, 131–314, 2005.

[2] Zou, W., W. Tang, J. Zhang, S. Luo, F. Liu, H. Zhang, Y. Luo, and T. J. Cui, "Dispersion compensation for spoof plasmonic circuits," *Progress In Electromagnetics Research*, Vol. 179, 95–100, 2024.

[3] Pitarke, J. M., V. M. Silkin, E. V. Chulkov, and P. M. Echenique, "Theory of surface plasmons and surface-plasmon polaritons," *Reports on Progress in Physics*, Vol. 70, No. 1, 1, 2007.

[4] Maier, S. A., *Plasmonics: Fundamentals and Applications*, Springer, New York, USA, 2007.

[5] Liu, H., B. Wang, L. Ke, J. Deng, C. C. Chum, S. L. Teo, L. Shen, S. A. Maier, and J. Teng, "High aspect subdiffraction-limit photolithography via a silver superlens," *Nano Letters*, Vol. 12, No. 3, 1549–1554, 2012.

[6] Xu, H., F. Nian, J. Deng, and M. Gao, "Compact broadband low-pass filter with novel fishbone structure based on spoof surface plasmon polariton," *Progress In Electromagnetics Research M*, Vol. 123, 95–103, 2024.

[7] Atwater, H., A. Polman, E. Kosten, D. Callahan, P. Spinelli, *et al.*, "Nanophotonic design principles for ultrahigh efficiency photovoltaics," in *AIP Conference Proceedings*, Vol. 1519, No. 1, 17–21, 2013.

[8] Zhuang, K., J.-P. Geng, Z. Ding, X. Zhao, W. Ma, H. Zhou, C. Xie, X. Liang, and R.-H. Jin, "A compact endfire radiation antenna based on spoof surface plasmon polaritons in wide bandwidth," *Progress In Electromagnetics Research M*, Vol. 79, 147–157, 2019.

[9] Zhang, S., Y. Xiong, G. Bartal, X. Yin, and X. Zhang, "Magnetized plasma for reconfigurable subdiffraction imaging," *Physical Review Letters*, Vol. 106, No. 24, 243901, 2011.

[10] Anker, J. N., W. P. Hall, O. Lyandres, N. C. Shah, J. Zhao, and R. P. V. Duyne, "Biosensing with plasmonic nanosensors," *Nature Materials*, Vol. 7, No. 6, 442–453, 2008.

[11] Quaranta, G., G. Basset, O. J. F. Martin, and B. Gallinet, "Recent advances in resonant waveguide gratings," *Laser & Photonics Reviews*, Vol. 12, No. 9, 1800017, Sep. 2018.

[12] Al-Gburi, A. J. A., I. Ibrahim, Z. Zakaria, and A. D. Khaleel, "Bandwidth and gain enhancement of ultra-wideband monopole antenna using MEBG structure," *ARPN Journal of Engineering and Applied Sciences (JEAS)*, Vol. 14, 3390–3393, 2019.

[13] Hibbins, A. P., B. R. Evans, and J. R. Sambles, "Experimental verification of designer surface plasmons," *Science*, Vol. 308, No. 5722, 670–672, 2005.

[14] Yao, K. and Y. Liu, "Plasmonic metamaterials," *Nanotechnology Reviews*, Vol. 3, No. 2, 177–210, 2014.

[15] Garcia-Vidal, F. J., L. Martín-Moreno, and J. B. Pendry, "Surfaces with holes in them: New plasmonic metamaterials," *Journal of Optics A: Pure and Applied Optics*, Vol. 7, No. 2, S97, 2005.

[16] Shen, X., T. J. Cui, D. Martin-Cano, and F. J. Garcia-Vidal, "Conformal surface plasmons propagating on ultrathin and flexible films," *Proceedings of the National Academy of Sciences*, Vol. 110, No. 1, 40–45, Jan. 2013.

[17] Tian, D., R. Xu, W. Li, Z. Xu, and A. Zhang, "Endfire antenna based on spoof surface plasmon polaritons," *Progress In Electromagnetics Research C*, Vol. 77, 11–18, 2017.

[18] Ma, H. F., X. Shen, Q. Cheng, W. X. Jiang, and T. J. Cui, "Broadband and high-efficiency conversion from guided waves to spoof surface plasmon polaritons," *Laser & Photonics Reviews*, Vol. 8, No. 1, 146–151, Jan. 2014.

[19] Pan, B. C., Z. Liao, J. Zhao, and T. J. Cui, "Controlling rejections of spoof surface plasmon polaritons using metamaterial particles," *Optics Express*, Vol. 22, No. 11, 13 940–13 950, 2014.

[20] Gao, X., L. Zhou, Z. Liao, H. F. Ma, and T. J. Cui, "An ultra-wideband surface plasmonic filter in microwave frequency," *Applied Physics Letters*, Vol. 104, No. 19, 191603, 2014.

[21] Cheng, Z. W., M. Wang, Z. H. You, H. F. Ma, and T. J. Cui, "Spoof surface plasmonics: Principle, design, and applications,"

Journal of Physics: Condensed Matter, Vol. 34, No. 26, 263002, 2022.

[22] Pendry, J. B., L. Martin-Moreno, and F. J. Garcia-Vidal, "Mimicking surface plasmons with structured surfaces," *Science*, Vol. 305, No. 5685, 847–848, 2004.

[23] Hibbins, A. P., B. R. Evans, and J. R. Sambles, "Experimental verification of designer surface plasmons," *Science*, Vol. 308, No. 5722, 670–672, 2005.

[24] Rusina, A., M. Durach, and M. I. Stockman, "Theory of spoof plasmons in real metals," *Applied Physics A*, Vol. 100, 375–378, 2010.

[25] Gao, X., J. H. Shi, X. Shen, H. F. Ma, W. X. Jiang, L. Li, and T. J. Cui, "Ultrathin dual-band surface plasmonic polariton waveguide and frequency splitter in microwave frequencies," *Applied Physics Letters*, Vol. 102, No. 15, 151912, 2013.

[26] Zhang, W., G. Zhu, L. Sun, and F. Lin, "Trapping of surface plasmon wave through gradient corrugated strip with underlayer ground and manipulating its propagation," *Applied Physics Letters*, Vol. 106, No. 2, 021104, 2015.

[27] Tang, W., J. Wang, X. Yan, J. Liu, X. Gao, L. Zhang, and T. J. Cui, "Broadband and high-efficiency excitation of spoof surface plasmon polaritons through rectangular waveguide," *Frontiers in Physics*, Vol. 8, 582692, 2020.

[28] Ma, H. F., X. Shen, Q. Cheng, W. X. Jiang, and T. J. Cui, "Broadband and high-efficiency conversion from guided waves to spoof surface plasmon polaritons," *Laser & Photonics Reviews*, Vol. 8, No. 1, 146–151, 2014.

[29] Jaiswal, R. K., N. Pandit, and N. P. Pathak, "Spoof surface plasmon polaritons based reconfigurable band-pass filter," *IEEE Photonics Technology Letters*, Vol. 31, No. 3, 218–221, 2018.

[30] Chaparala, R. and S. Tupakula, "Metal-insulator-metal structured surface plasmon polariton waveguide with improved gain."

[31] Ghattas, N., A. M. Ghuniem, and S. M. Abuelenin, "Optimization of dielectric rod antenna design in millimeter wave band for wireless communications," *ArXiv Preprint ArXiv:1805.05475*, 2018.

[32] Reese, R., H. Tesmer, E. Polat, M. Jost, M. Nickel, R. Jakoby, and H. Maune, "Fully dielectric rod antenna arrays with high permittivity materials," in *2019 12th German Microwave Conference (GeMiC)*, 13–16, Stuttgart, Germany, Mar. 2019.

[33] Al-Gburi, A. J. A., I. Ibrahim, and Z. Zakaria, "Band-notch effect of u-shaped split ring resonator structure at ultra wideband monopole antenna," *International Journal of Applied Engineering Research*, Vol. 12, No. 15, 4782–4789, 2017.

[34] Kazemi, R., A. E. Fathy, and R. A. Sadeghzadeh, "Dielectric rod antenna array with substrate integrated waveguide planar feed network for wideband applications," *IEEE Transactions on Antennas and Propagation*, Vol. 60, No. 3, 1312–1319, 2012.

[35] Withayachumnankul, W., R. Yamada, M. Fujita, and T. Nagatsuma, "All-dielectric rod antenna array for terahertz communications," *APL Photonics*, Vol. 3, No. 5, 051707, 2018.

[36] Jaiswal, R. K., N. Pandit, and N. P. Pathak, "Design, analysis, and characterization of designer surface plasmon polariton-based dual-band antenna," *Plasmonics*, Vol. 13, 1209–1218, 2018.

[37] Zheng, Y., Z. Wang, Z. Li, Y. Sha, Z. Jiang, and L. Nie, "A spoof surface plasmon polariton antenna feeding with horn," in *2021 IEEE MTT-S International Microwave Workshop Series on Advanced Materials and Processes for RF and THz Applications (IMWS-AMP)*, 30–32, Chongqing, China, Nov. 2021.

[38] Cao, D., Y. Li, and J. Wang, "A millimeter-wave spoof surface plasmon polaritons-fed microstrip patch antenna array," *IEEE Transactions on Antennas and Propagation*, Vol. 68, No. 9, 6811–6815, 2020.

[39] Cao, D., Y. Li, J. Wang, and L. Ge, "A millimeter-wave spoof-surface-plasmon-polaritons-fed dual-polarized microstrip patch antenna array," *IEEE Transactions on Antennas and Propagation*, Vol. 71, No. 3, 2363–2374, 2023.

[40] Zhang, Y., S. Lin, B. Zhu, J. Cui, Y. Mao, J. Jiao, and A. Denisov, "Broadband and high gain dielectric-rod end-fire antenna fed by a tapered ridge waveguide for K/Ka bands applications," *IET Microwaves, Antennas & Propagation*, Vol. 14, No. 8, 743–751, 2020.

[41] Saffold, G. L. and T. M. Weller, "Dielectric rod antenna array with planar folded slot antenna excitation," *IEEE Open Journal of Antennas and Propagation*, Vol. 2, 664–673, 2021.

[42] Ahmadi, E., S. Fakhte, and S. S. Hosseini, "Dielectric rod nanoantenna fed by a planar plasmonic waveguide," *Optical and Quantum Electronics*, Vol. 55, No. 2, 115, 2023.

[43] Fakhte, S., "A new planar feeding method of dielectric rod antenna using dielectric resonator," *Scientific Reports*, Vol. 13, No. 1, 9242, 2023.